3-D NUMERICAL SIMULATION OF TURBULENT STRUCTURE IN TIME-DEPENDENT AND DEPTH-VARYING UNSTEADY COMPOUND OPEN CHANNEL FLOWS

Iehisa Nezu
Department of Civil and Global Environment Engineering, Kyoto University
Kyoto, 606-8501, Japan
nezu@nezu.gee.kyoto-u.ac.jp

Michio Sanjou
Department of Civil and Global Environment Engineering, Kyoto University
Kyoto, 606-8501, Japan
sanjou@nezu.gee.kyoto-u.ac.jp

ABSTRACT

There are a lot of previous studies on compound open-channel flows, because such a two-stage flow with a lower main-channel and floodplains is one of the most important flows for water disaster prevention, valuable open-spaces of aquatic lives and river ecosystems. However, there are quite few studies on three-dimensional (3-D) structures in depth-varying unsteady compound open-channel flows. In this study, a 3-D time-dependent numerical model is developed and applied to such unsteady depth-varying compound free-surface flows. The calculated results are compared with the reliable experimental database of LDA, and the unsteadiness properties of mean velocity and turbulence structures are discussed in detail.

INTRODUCTION

Compound open-channel flows are often observed in many rivers. They consist of main-channel and floodplains. As the difference of mean velocities between the main-channel and floodplains becomes larger at the junction, it promotes secondary currents and turbulent transport of various scalars such as sediment transport in the spanwise direction. Therefore, it is necessary in hydraulic engineering and river environment to investigate the turbulent structure in compound open-channel flows. With the development of computer systems, some complicated numerical simulations are now available. For example, Kawahara & Tamai(1988) and Naot *et al.*(1993) have calculated some steady depth-fixed compound open-channel flows by using an algebraic stress model(ASM), and reproduced the distributions of mean flow, secondary currents and turbulence. Cokljat & Younis(1995) have applied a complete Reynolds-stress model(RSM) and reproduced the main features in compound channels. Thomas & Williams (1995) have calculated the primary velocity profiles and the wall shear stress by using a large eddy simulation (LES). Hosoda *et al.*(1999) have reproduced the physical relation of secondary currents and horizontal coherent eddies by using a non-linear $k-\varepsilon$ model. Sofialidis & Prinos(1999) have simulated the flow structure in the whole region from the near-wall to free surface by using a low-Reynolds-number and non-linear $k-\varepsilon$ model.

However, these above-mentioned studies deal with not unsteady but steady compound open-channel flows. In fact, when depth-varying flooded rivers are considered in time, it is quite needed to examine the hydrodynamic characteristics in time-dependent and depth-varying unsteady compound open-channel flows. Recently, Nezu *et al.* (2002) have conducted some turbulence measurements in unsteady compound open-channel flows by using a laser Doppler anemometer(LDA), and found the time-variations of the wall shear stress and the typical secondary currents in the main-channel and floodplain. In this study, 3-D time-dependent numerical model was developed and applied to such an unsteady depth-varying compound free-surface flow. The computed values were compared with the existing experimental results of LDA, and it was found that the present numerical model is able to reproduce the unsteadiness properties of secondary flows, primary mean velocity and turbulence structures.

BASIC EQUATIONS AND NUMERICAL MODELING

Fig.1 shows the coordinate system of the present calculation, in which coordinates x, y and z are the streamwise, vertical and spanwise, respectively. The ensemble-averaged velocity components in each direction are defined as U, V, W and the turbulence components are defined as u, v, w, respectively.

The continuity and RANS equations are described in the followings.

(continuity equation)

$$\frac{\partial U}{\partial x}+\frac{\partial V}{\partial y}+\frac{\partial W}{\partial z}=0 \tag{1}$$

(RANS equation)

$$\frac{DU_i}{Dt}=-\frac{1}{\rho}\frac{\partial(P+\Omega)}{\partial x_i}+\frac{\partial}{\partial x_j}\left(\nu\frac{\partial U_i}{\partial x_j}-\overline{u_i u_j}\right) \quad (i=1,2,3) \tag{2}$$

Table 1: Calculation cases

case	H_b (cm)	H_p (cm)	B_f/B	H_b/D	H_p/D	Q_b (l/s)	Q_p (l/s)	Um_b (cm/s)	Um_p (cm/s)	T_d (s)	α ($\times 10^{-3}$)
HH60	7.5	10.5	0.5	1.5	2.1	2.1	14.4	10.5	45.0	60	1.80
HH120	7.5	9.5	0.5	1.5	1.9	2.1	7.3	10.5	26.0	120	0.91

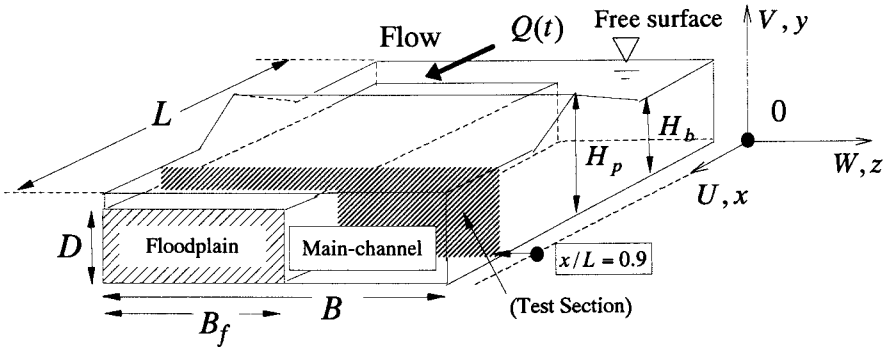

Fig.1: Calculation region and coordinate system

Ω is the gravity potential function and P is the mean pressure. The Reynolds stress $-\overline{u_i u_j}$ is calculated using the algebraic stress model (Eqs.(3)-(9)) proposed by Naot *et al.*(1993).

$$\overline{uv} = -\nu_{ty}\left(\frac{\partial U}{\partial y} + \frac{\partial V}{\partial x}\right) \tag{3}$$

$$\overline{uw} = -\nu_{tz}\left(\frac{\partial U}{\partial z} + \frac{\partial W}{\partial x}\right) \tag{4}$$

$$\overline{vw} = \frac{\alpha_2}{(C_1 + \frac{3}{2}C_3)}\frac{k}{\varepsilon}\left(\overline{uw}\frac{\partial U}{\partial y} + \overline{uv}\frac{\partial U}{\partial z}\right) - C_\mu \frac{k^2}{\varepsilon}\left(\frac{\partial W}{\partial y} + \frac{\partial V}{\partial z}\right) \tag{5}$$

$$\overline{v^2} = \frac{k}{(C_1 + 2C_3)}\left[\frac{2}{3}\left(\alpha_1 - \frac{1}{2}\alpha_2 + C_1 - 1\right) + \frac{\alpha_2}{\varepsilon}\left(\overline{uv}\frac{\partial U}{\partial y} - \overline{uw}\frac{\partial U}{\partial z}\right)\right] - 2C_\mu \frac{k^2}{\varepsilon}\frac{\partial V}{\partial y} \tag{6}$$

$$\overline{w^2} = \frac{k}{C_1}\left[\frac{2}{3}\left(\alpha_1 - \frac{1}{2}\alpha_2 + C_1 - 1\right) + \frac{\alpha_2}{\varepsilon}\left(\overline{uw}\frac{\partial U}{\partial z} - \overline{uv}\frac{\partial U}{\partial y}\right) + C_3\frac{\overline{v^2}}{k}\right] - 2C_\mu \frac{k^2}{\varepsilon}\frac{\partial W}{\partial z} \tag{7}$$

$$\nu_{ty} = \frac{C_1^2}{(C_1 + \frac{3}{2}C_3)(C_1 + 2C_3)} C_\mu \frac{k^2}{\varepsilon} \tag{8}$$

$$\nu_{tz} = \frac{(C_1 + \frac{5}{2}C_3)}{(C_1 + 2C_3)} C_\mu \frac{k^2}{\varepsilon} \tag{9}$$

C_1, C_3, α_1 and α_2 are the model coefficients. They are given by

$C_1 = 1.50 - 0.50 f_1$, $C_3 = 0.10 f_2$, $\alpha_1 = 0.7636 - f_1$, $\alpha_2 = 0.1091 + f_1$ and $C_\mu = 0.09 f_t$,

in which, f_1 and f_2 are the damping functions that were proposed by Naot *et al.*(1993).

$$f_1 = \left(\frac{l}{y_a}\right)^2, \quad f_2 = \left(\frac{l}{h_a}\right)^2, \quad l = \left(\frac{C_\mu^{3/4}}{\kappa}\right)\frac{k^{3/2}}{\varepsilon}$$

$$y_a = \left(\frac{1}{y^2}\right)^{-1/2} \text{ and } h_a = \left[\frac{1}{(H-y)^2}\right]^{-1/2} + 0.3162l$$

f_t is a function of unsteadiness parameter that was proposed by Nezu & Sanjou(2002).

VOF(volume of fluid) method was applied here to the calculation of free surface. This VOF, which was proposed by Hurt & Nichols (1981), is an effective method for analysis of time-dependent free-surface elevation. In this method, the VOF function F is used, which means a fluid-existing rate of one calculation cell. The shape of free surface is determined by solving the following convection equation.

$$\frac{\partial F}{\partial t} + \frac{\partial U_i F}{\partial x_i} = 0, \qquad (0 \le F \le 1) \tag{10}$$

These governing equations of (1) to (10) were calculated by a finite-differential method. The number of grid is 300×25×40 in (x, y, z) and their cell sizes $(\Delta x, \Delta y, \Delta z)$ in each direction are $\Delta x = 1.5$ cm, $\Delta y = 0.5$ cm and

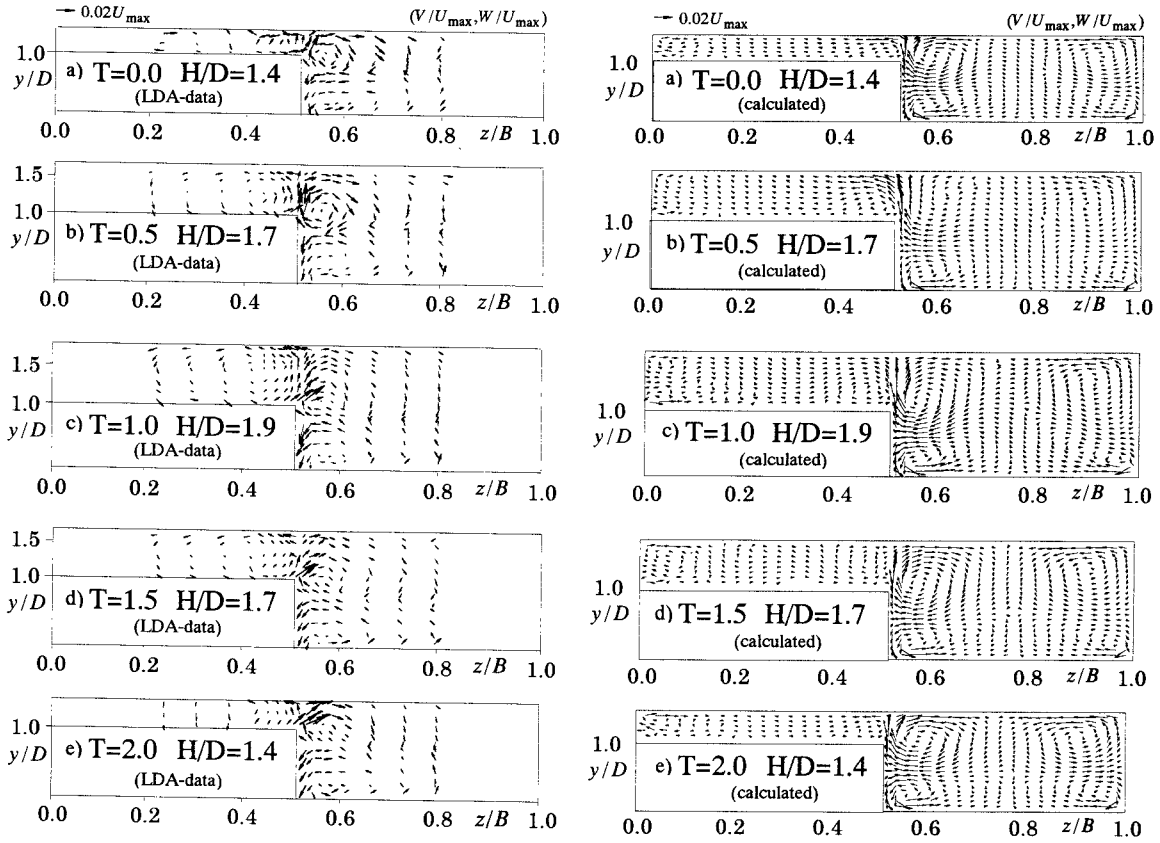

Fig.2: Distributions of secondary currents (V, W) as a function of time $T \equiv t/T_d$ for case HH60

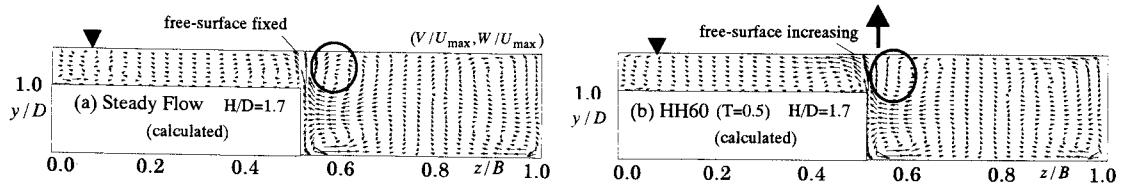

Fig.3: Comparison of secondary current between steady and unsteady flows

$0.75 \le \Delta z \le 1.25$ cm respectively.

The primary velocity $U(t)$ and the water depth $H(t)$ at the channel entrance were given as sine curves that are the function of time. The log-law was applied for the velocity calculation at the first point in the wall region and the free conditions were imposed at the outflow section of $x = L$ (see Fig.1).

APPLICATION TO DEPTH-VARYING UNSTEADY FREE SURFACE FLOW

The validity of the present computational method is examined to compare with the experimental results of 3-D LDA measurements by Nezu *et al.* (2002). Table 1 shows these hydraulic conditions, in which H is the water depth in the main-channel, B and B_f are the channel width and the floodplain width, respectively. D is the floodplain height. Um is the bulk mean velocity. T_d is the duration time from the base depth to the peak depth of flooded flow.

The subscripts b and p denote the base and peak flows, respectively. α is the unsteadiness parameter of Nezu & Nakagawa(1991)and it is defined as

$$\alpha = \frac{1}{(Um_b + Um_p)/2} \frac{H_p - H_b}{T_d} \qquad (11).$$

In this paper, two kinds of calculation cases were treated. As α becomes larger, the flow unsteadiness is stronger. That is to say, case HH60 has larger unsteadiness than HH120. The test section was located at $x/L = 0.9$ (see Fig.1). L is the calculation length in the streamwise direction. In the present calculations, L was chosen to be twenty times the main-channel depth H_b at base flow, i.e., $L = 20H_b$. The numerical results shown in the following sections are the values at this test section.

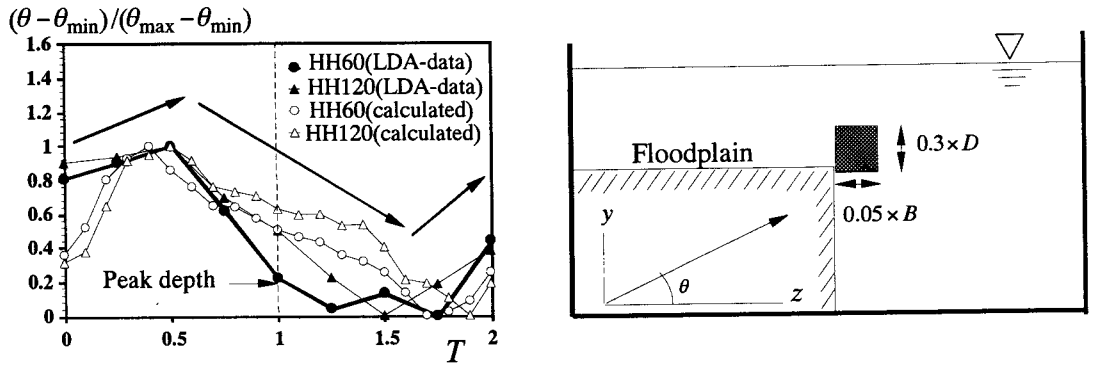

Fig.4: Time-variation of secondary flow from the junction-edge toward free-surface

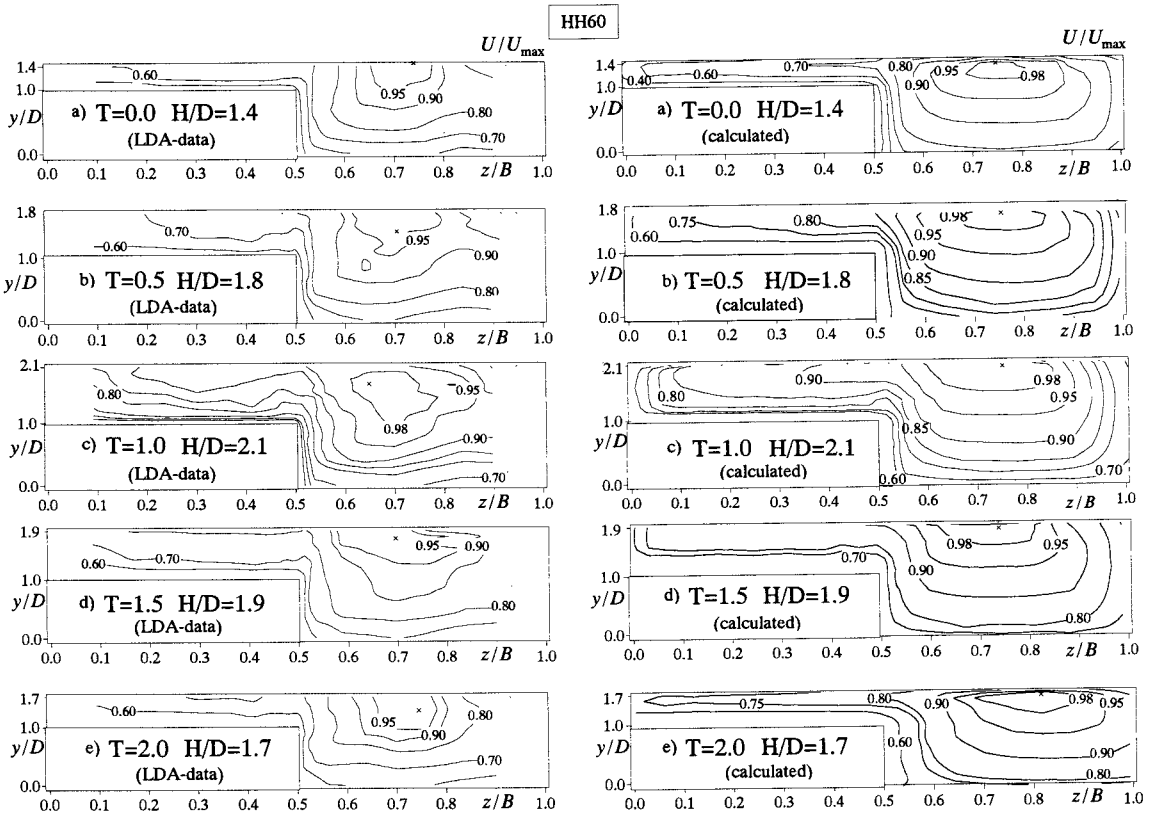

Fig.5: Isovel lines of primary velocity in the cross section, (HH60).
(The symbol x means the position of the maximum velocity)

RESULTS AND DISCUSSIONS

Time-Variations of Secondary Currents

Fig.2 shows the velocity vector descriptions of the secondary currents normalized by the maximum mean velocity U_{max}. In this figure, both the experimental and calculated values are indicated at the typical phase time of flood, that is, as a function of the time $T \equiv t/T_d$ which is normalized by the duration time T_d. This means that $T = 0.0$ is a steady stage before the beginning of change of discharge $Q(t)$. The time of $0 < T < 1.0$ is the rising stage of flood, and the water depth attains a peak at $T = 1.0$. The time of $1.0 < T < 2.0$ is the falling stage, and the flow returns to the base flow at $T = 2.0$. In all stages, typical secondary currents are observed clearly. These secondary currents are the same manner as those in steady compound channel flows of Naot *et al.*(1993). The flow direction of secondary currents from the junction edge toward the free surface of main-channel becomes almost vertical in the rising stage($T = 0.5$). From these figures, it is found that the present calculation model can reproduce well the unsteadiness features of secondary currents measured by LDA.

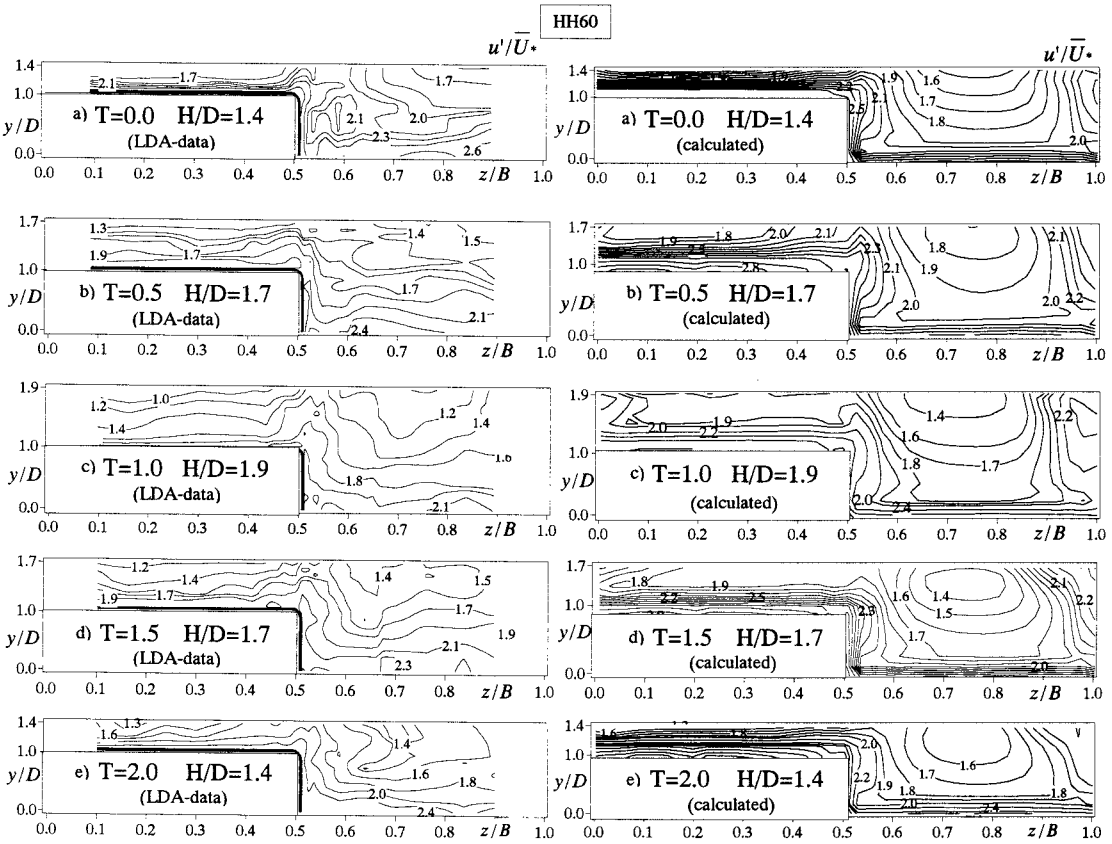

Fig.6: Contours of turbulence intensity $u'/\overline{U_*}$ against time, (HH60)

Fig.3 shows the comparison of secondary currents between (a)steady flow and (b)unsteady rising (at $T = 0.5$ for HH60) one. The steady case(a) was calculated under the same depth and discharge conditions as the unsteady case (b). From this figure, it is recognized that the rising water depth makes the vector angle of secondary flow near the junction almost vertical.

Fig.4(left-hand-side) shows the time-variations of the vector angle θ in the secondary flow from the junction edge toward the free surface. θ is a space-averaged value in the finite region indicated in Fig.4(right-hand-side). It is found that the vector angle θ increases in the rising stage and decreases in the falling stage. This feature is more remarkable as the unsteadiness is larger in both the measured and computed results.

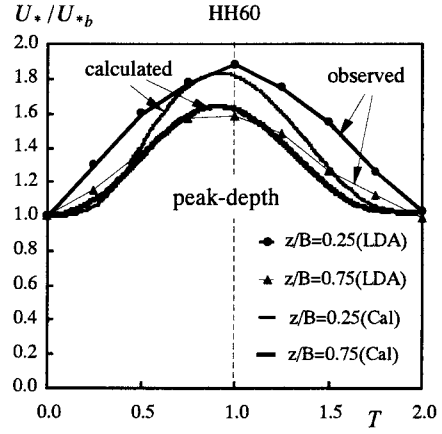

Fig.7: Time-variation of friction velocity(HH60)

Distributions of Primary Velocity against Time

Fig.5 shows the distributions of the normalized primary velocity U/U_{max} as a function of time in the case of HH60. In these figures, there are bulge patterns from near the junction toward free surface. This bulge feature is also observed in steady compound channels. At the base-depth time($T = 0$), the velocity in the main-channel is much larger than that over the floodplain. As the floodplain depth increases with time, the differences of velocities between the main-channel and floodplain become smaller.

Turbulence Structure in the Unsteady Compound Open-Channel Flow

Fig.6 shows the time-dependent contours of turbulence intensity u' in the streamwise direction. u' is defined as

$$u' \equiv \sqrt{u^2} \qquad (12).$$

These values are normalized by the averaged friction velocity $\overline{U_*}$ in the case of HH60.

In all time-stages, u' becomes larger near the junction and there are same bulge patterns as observed in the distributions of mean velocity U (see Fig.5). It should be noticed that the secondary currents have a significant influence on not only mean velocity but also turbulence characteristics.

Distributions of Wall Shear Stress

Fig.7 is the time-variation of the friction velocity U_* on the main-channel $(z/B = 0.75)$ and flood plain $(z/B = 0.25)$. These values are normalized by the base flow value U_{*b}. In both the calculated and LDA values, U_* increases more rapidly on the floodplain than in the main-channel. It is found that the present calculations can reproduce well the time-dependent friction characteristics in unsteady two-stage flows.

Fig.8 shows the spanwise distributions of wall shear stress $\tau_w \equiv \rho U_*^2$. These values are normalized by the averaged value $\overline{\tau}_{w,b}$ along the perimeter. In all typical stages, τ_w decreases locally near the junction edge. At the base depth stage $(T = 0)$, τ_w is larger in the main-channel than the floodplain. With an increase of water depth $H(t)$, τ_w on the floodplain increases rapidly and becomes larger on floodplain rather than on main-channel.

CONCLUDING REMARKS

A numerical simulation was conducted in depth-varying unsteady compound open-channel flows by using ASM and VOF. It was found that the present model was able to reproduce the 3-D unsteadiness properties of primary velocity, secondary currents and wall shear stress. The main findings in this study are as follows:

1)The present numerical model reproduced well the time-dependent distributions of the mean velocity and turbulence intensity observed in LDA database.

2) Time dependent properties in the secondary flow could be reproduced. The angle of the secondary flow from the junction edge toward the free-surface increases and decreases in the rinsing and falling stages, respectively.

3)The wall shear stress τ_w is larger on the main-channel than on the floodplain at the base flow. With an increase of the floodplain depth, the value of τ_w on floodplain becomes much larger.

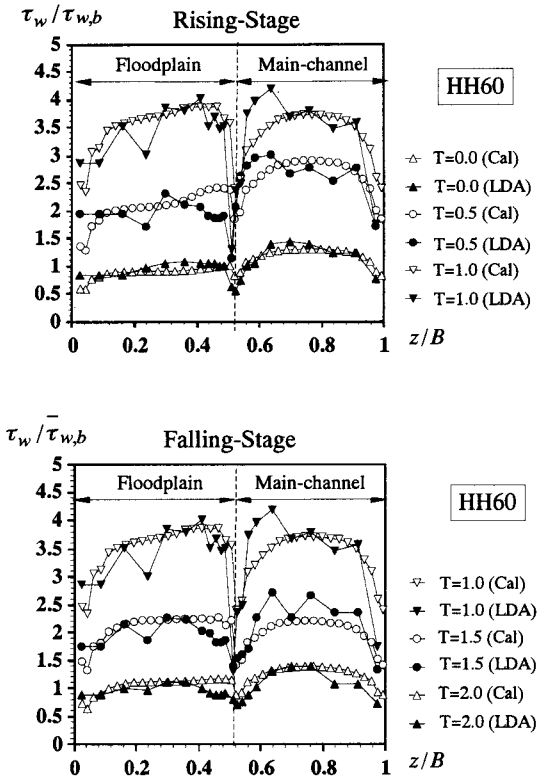

Fig.8: Distributions of wall-shear stress
(Upper : Rising-stage, Lower : Falling-stage)

References

Cokljat, D. and Younis, B.A, 1995, "Compound-channel flows, a parametric study using a Reynolds-stress transport closure", *J. of Hydraulic Res.*, IAHR, Vol.33, No.3, pp.307-320.

Hosoda, T., Sakurai, T., Kimura, I. and Muramoto, Y., 1999, "3-D computations of compound open channel flows with horizontal vortices and secondary currents by means of non-linear $k-\varepsilon$ model", *J. of Hydroscience and Hydraulic Eng.*, JSCE, Vol.17, No.2, pp.87-96.

Hurt, C.W. and Nichols, B.D., 1981, " Volume of fluid method for the dynamics of free boundaries", *J. of Comp. Phys.*, Vol.39, pp.201-225.

Kawahara, Y. and Tamai, N., 1988, "Numerical calculation of turbulent flows in compound channels with an algebraic stress turbulence model", *Proc. of 3rd Int. Symp. on Refined Flow Modeling and Turbulence Measurement*, pp.9-16.

Naot, D., Nezu, I. and Nakagawa, H., 1993, "Hydrodynamic behavior of compound rectangular open-channel flows", *J. of Hydraulic Eng.*, ASCE, Vol.119, pp.390-408.

Nezu, I., Kadota, A. and Nakagawa, H., 1997, "Turbulent structure in unsteady depth-varying open-channel Flows", *J. of Hydraulic Eng.*, ASCE, Vol. 123, pp.752-763.

Nezu, I. and Sanjou, M., 2002, "Numerical calculation of near-wall region in unsteady open-channel flows", *Advances in Hydraulics and Water Engineering (ed. J.J. Guo)*, World Scientific Pub., Vol.1, pp.136-142.

Nezu, I., Sanjou, M. and Sakane, Y., 2002, "Three-dimensional measurements with laser Doppler anemometers in unsteady depth-varying compound open-channel flows", *Advances in Hydraulics and Water Engineering (ed. J.J. Guo)*, World Scientific Pub., Vol.1, pp.56-61.

Sofialidis, D. and Prinos, P., 1999, "Numerical study of momentum exchange in compound open channel flow", *J. of Hydraulic Eng.*, ASCE, Vol.125, pp.152-165.

Thomas, T.G. and Williams, J.J.R., 1995, "Large eddy simulation of turbulent flow in an asymmetric compound open-channel", *J. of Hydraulic Res.*, IAHR, Vol.33, No.1, pp.27-41.